INHERENT OPTICAL PROPERTIES OF THE AEROSOLS FOR OLCI/SENTINEL-3: FROM MICRO-PHYSICAL PROPERTIES TO OPTICAL PROPERTIES USING AERONET

***Richard Santer*[(1,4)], *Francis Zagolski*[(1,2)], *and Ouahid Aznay*[(1,3)]**

[(1)] *ADRINORD, Association pour le Développement de la Recherche et de l'Innovation dans le bassin du Nord-Pas-de-Calais, 2 rue des Cannoniers, F59000, Lille – FRANCE. E-mail: Santer.Richard@yahoo.fr*

[(2)] *PARBLEU Technologies Inc., 79 Veilleux street, St Jean-sur-Richelieu (QC), J3B-3W7 – CANADA. E-mail: Francis_Zagolski@yahoo.ca*

[(3)] *C-S Systèmes d'Information, ZAC de la Grande Plaine, F31506-Toulouse - FRANCE 31506 E-mail: Ouahid.Aznay@c-s.fr*

[(4)] *E-mail: Université du Littoral Cote d'Opale, MREN, 32 Avenue Foch, F62930 Wimereux, FRANCE santer@univ-littoral.fr*

ABSTRACT

A well-knowledge of the aerosol optical properties (AOPs) is a strong requirement for achieving the atmospheric correction over ocean. Since several decades, these AOPs were computed with standard aerosol models (SAMs) characterized by their micro-physical properties. From the characteristics of microphysics can be derived the inherent optical properties (IOPs). These SAMs were still used in the generation of the MERIS (Medium Resolution Imaging Spectrometer) auxiliary data file (ADFs) to feed the atmospheric correction algorithm. This approach has been recently revisited by using models derived from the analysis of the AERONET (AErosol RObotic NETwork) measurements [1]. Alternatively, IOPs of these aerosols could be directly extracted from these AOPs [2].

These two approaches are compared by starting to build a database with aerosol IOPs over four AERONET stations in the Northern Sea plus one at AAOT (Acqua Alta Oceanographic Tower, Venice - Italy). Several thousands of data sequences with aerosol IOPs were processed with filtering techniques and statistical methods to produce 16 classes of aerosols. An analysis of the dispersion of the IOPs in each class will be conducted first, to translate this dispersion into an error on the aerosol model extracted in the near-infrared domain from space. Second, we will evaluate how well the aerosol reflectance can be predicted in the visible region in the frame of the ocean colour observation. The first objective will consist in a direct comparison between the two approaches to derive the IOPs of the aerosols from AERONET.

Moreover, the need to account for a seasonal and regional variability of the aerosol models will be analyzed, as well the potential that can offers a bi-angular viewing geometry (such as with AATSR, Advanced Along-Track Scanning Radiometer) in a finer identification of the aerosol IOPs. The possible consequence of the OLCI/Sentinel-3 tilt on the characterization of the aerosols will be finally discussed.

1 INTRODUCTION

They are different approaches in the use of one AERONET data which combines at a given time multi spectral measurements of the extinction of the solar beam and of the sky radiance field:

(i) A direct transformation of the sky radiance into the aerosol phase function under the name of WOPAER [2].

(ii) The AERONET team proposes a micro physical description of the aerosols through the retrieval of standard size distributions of the aerosols associated to the aerosol refractive index [3]. This micro physical description is available on the AERONET web server. We will denominate this approach AERONR.

(iii) This AERONET micro-physical description is used to compute the aerosol phase function at 3 wavelengths (440 nm, 670 nm and 870 nm). We will denominate this approach AEROPA.

The individual sets of IOPS can be used to generate aerosol climatology. It was done:

(i) At a global scale for MERIS with WOPAER both over the land [4] and over the ocean [5].

(ii) For MODIS and SeaWiFS using AERONR over the ocean [6] at a global scale but accounting from the seasonal variability.

Because a direct link exists between AERONR and AEROPA, we can foresee that aerosol climatology conducted with the two will be compatible.

Section 2 will include the description of the AERONET measurements we used, the methodology we applied to realize the classes of IOP in the three CIMEL spectral bands, the tools we used to generate the MERIS aerosol models (MAM). This generation of the MAMs will be done for the 2Seas region using AEROPA but also in the AERONET station of shore of Venice (AAOT). The AAOT is a reference station

for the MERIS validation and it will be used to evaluate the evolution of the atmospheric correction when using different sets of MAM. Section 3 is similar to section 2 but for WOPAER. In section 4, we will discuss the perspectives with S3.

2. THE AEROSOL OPTICAL PROPERTIES FROM AEROPA

2.1) The AERONET data base

A data base of aerosol optical thickness (AOT) and phase functions is available in the AERONET web server. Table 1 gives for each AERONET station the number of individual measurement file with: N1: total number of sequences of the aerosol phase functions, N2: same as N1 but with the single scattering albedo.

Site	N1	N2	Site	N1	N2
Dunkerque	1096	173	RameHead	10	0
Helgoland	520	44	De Hague	528	89
Lannion	37	5	AAOT	5362	837
Oostende	1468	104	Total	9021	1252

Table 1: Number of sequences per station as described above for AEROPA

On a practical point of view, when we do not have a value of the single scattering albedo (SSA), it means that only the forward scattering radiance and the AOT are used to determine the aerosol model. When the SAS is provided, it means that the radiance in backscattering has been used.

2.2 –Ordering the AEROPA data base versus the Angstroem coefficient in the NIR

The selection of the aerosol model is based on the spectral dependence of the aerosol reflectance. Therefore, we want to organize the data base versus the Angstroem coefficient in the NIR, defined as:

$$\alpha(\lambda,\lambda') = \frac{\log(\tau_a(\lambda)/\tau_a(\lambda'))}{\log(\lambda/\lambda')}, \qquad (1)$$

The realisation of the data base is straightforward:

(i) We defined 16 classes in α(670 nm, 870 nm) starting at 0 with a step of 0.15.

(ii) For each class, we simply average α(670 nm, 870 nm), α(440 nm, 670 nm), the *SSA* and P_a. We also computed for each of them the *rms*.

The methodology will be evaluated with the AAOT data set which is the largest.

The dispersion of the aerosol phase function is quite important, here at 865 nm, and two scattering angles as illustrated in figure 1. It is not possible to describe with accuracy P_a, therefore (i) it is important to evaluate the impact of the poor knowledge of P_a on the water reflectance retrieval. An error bar can be generated through the use of maximum and minimum values of Pa and the spectral dependences of AOT. (ii) You cannot have an accurate value of AOT_865. A validation through AOT needs a significant number of matchups to be valid in mean.

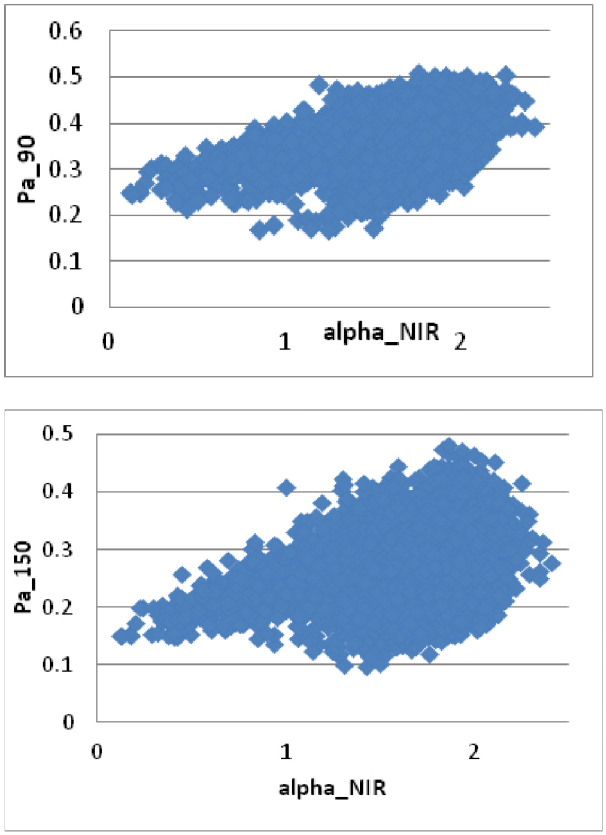

Figure 1: Aerosol phase function at 870 nm and in two scattering angles for the 3562 sequences

The performance of the AC has not to be judged on the retrieval of the AOT but on the possibility to predict ε

$$\varepsilon(\lambda,\lambda') = \frac{\log(\rho_a(\lambda)/\rho_a(\lambda'))}{\log(\lambda/\lambda')}, \qquad (2)$$

, the spectral dependance of the aerosol reflectance, in the blue from ε in the NIR. More excatly, we extract the aerosol reflectance in the NIR and we want to know it in the blue. The quality control is knowing the spectral dependenc of ε in the NIR how well do we know this spectral dependence in the blue? According to figure 2, starting from the knowledge of the spectral dependence of $\tau_a P_a$ in the NIR, we have a large dispersion in the prediction of $\tau_a P_a$ in the visible.

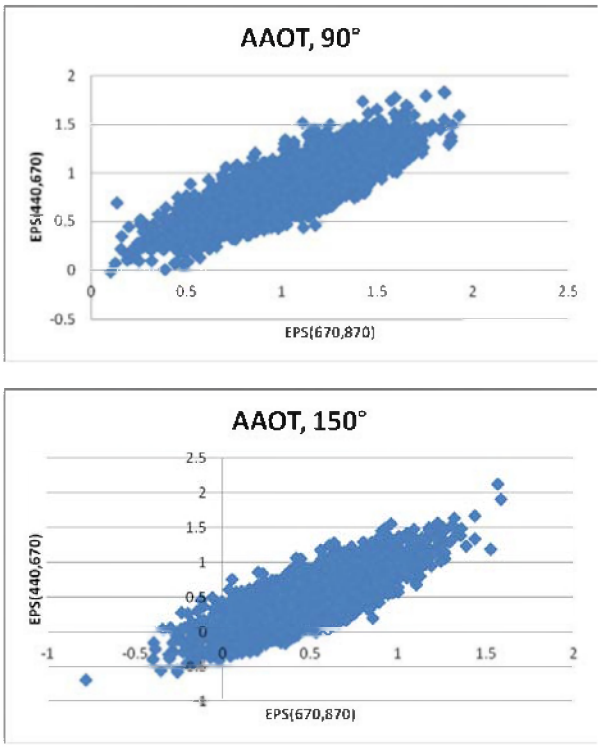

Figure 2: ε(440,670) versus ε(670,870) for two scattering angles

2.3 –The 16 classes of aerosol IOP

We defined 16 classes of IOPs to be in line with the number of standard aerosol models used for MERIS. The first model 1 is centred at α=0.15; the increment is d α =0.15 and the width of each class is 0.3.We also apply an iterative filter on Pa:
(i) At order 0, we compute the mean at the sigma for the 83 scattering angles and the three spectral bands.
(ii) In an iterative loop, for the scattering angle domain (30°, 150°), we exclude sequences for which the relative dispersion is greater than 25 percent.

Table 2 illustrates the AAOT classification. The two first classes are almost empty which renders difficult to define the aerosol IOP for these two classes. On the other hand, the probability to see these two classes during MERIS matchups is low.

class	center	N	alp_nir	alp_vis	class	center	N	alp_nir	alp_vis
1	0.00	2	0.12	0.22	9	1.20	525	1.19	1.45
2	0.15	9	0.20	0.33	10	1.35	846	1.33	1.51
3	0.30	42	0.36	0.56	11	1.50	1253	1.47	1.56
4	0.45	83	0.46	0.70	12	1.65	1758	1.61	1.62
5	0.60	122	0.60	0.88	13	1.80	1972	1.74	1.67
6	0.75	171	0.74	1.08	14	1.95	1401	1.86	1.74
7	0.90	228	0.89	1.25	15	2.10	554	1.98	1.83
8	1.05	319	1.04	1.35	16	2.25	119	2.10	1.93

Table 2: For each of the 16 class, we give the nominal centre in α, the number N of sequences per class, the Angstroem coefficients first between 670 nm and 870 nm; second between 440 nm and 670 nm.

The key parameter is *ε(870,440)* through the capability to extrapolate the aerosol path radiance from 870 nm to 440 nm, figure 4. 10 percent error on it directly results in 10 percent error on the retrieval of the aerosol reflectance in the blue following a single scattering approximation. The aerosol reflectance and the water reflectance in the visible are of the same order of magnitude. In other terms, in the AAOT it will be difficult to retrieve the water reflectance with accuracy better than 10 to 20 percent depending on the scattering angle. A vicarious adjustment may remove a bias but not the dispersion.

Fig. 3 also illustrates the difficulty to do atmospheric correction for small aerosols, actually in coastal waters compared to the larger aerosols found in the open ocean. First, the correction is larger and second because the error bars are also bigger.

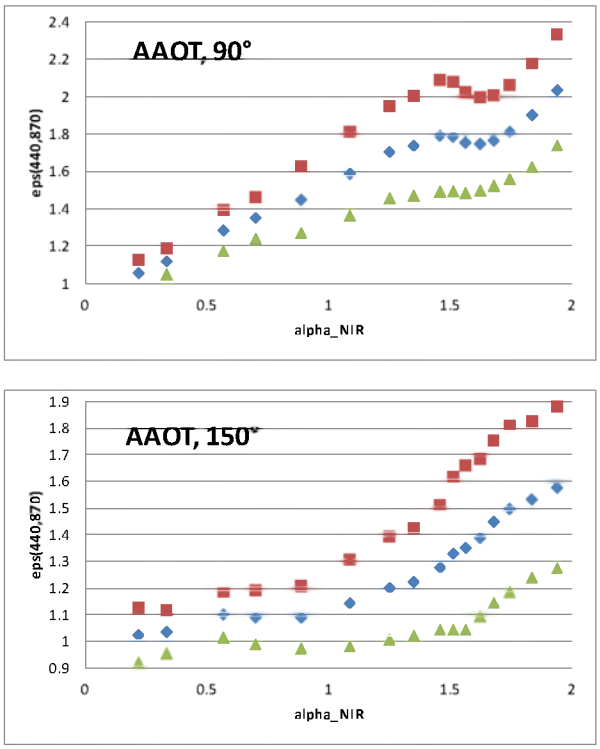

Figure 3: ε(440,870)for two scattering angles with the mean value (blue diamond), the maximum (red square) and minimum (green triangle) values at one sigma

2.4 –Seasonal variability

On the AAOT, for the class#12, we did two subsets: winter includes November, December, January, February and March; summer includes May, June, July, August and September. The two sets are comparable: (i) In AOT, table 3; (ii) In P_a, at least for the two selected scattering angles table 4. (iii) In ε, table 5. Within the dispersion, we cannot notice on any of the key aerosol IOPs any seasonal trend

This study may need to be consolidated for another AERONET stations for which the meteorology suggest the presence of seasonal wind regimes which may impact on the nature of the aerosols.

	lambda	440	670	870	alpha
Winter	mean	0.209	0.119	0.081	1.521
501	sigma	0.213	0.139	0.095	0.085
Summer	mean	0.240	0.123	0.084	1.509
722	sigma	0.199	0.124	0.085	0.086

Table 3: AOT (mean and sigma) in AAOT at 3 wavelengths and $\alpha(670,870)$

	90	120	150	90	120	150	90	120	150
mean	0.224	0.115	0.118	0.318	0.181	0.189	0.364	0.230	0.248
sigma	0.041	0.020	0.020	0.055	0.042	0.043	0.054	0.052	0.058
percent	18.4	17.2	16.6	17.3	23.3	22.7	14.9	22.6	23.4
mean	0.235	0.116	0.124	0.339	0.199	0.222	0.373	0.250	0.292
sigma	0.039	0.019	0.018	0.049	0.039	0.045	0.045	0.046	0.059
percent	16.5	16.1	14.4	14.4	19.5	20.1	12.2	18.5	20.2

Table 4: P_a (mean and sigma) in AAOT at 3 wavelengths and 3 scattering angles: winter (above) and summer (below)

	90	120	149
mean	1.70	1.40	1.36
sigma	0.28	0.25	0.35
percent	16.37	17.96	25.98
mean	1.87	1.40	1.28
sigma	0.28	0.23	0.28
percent	15.24	16.31	21.86

Table 5: same as Tab. 5 but for $\varepsilon(440,870)$

2.4 –Regional variability

We now consider the two data sets: AAOT and 2seas. Figure 4 compares P_a at 440 nm. To indicate the dispersion of P_a, we plotted both P_a and $P_a + \sigma P_a$ a in order to illustrate the dispersion. Of course by symmetry, we can imagine what $P_a - \sigma P_a$ is. Clearly, the two sets differ but the dispersion is such that it is difficult to promote a regionalisation of the aerosols for this case.

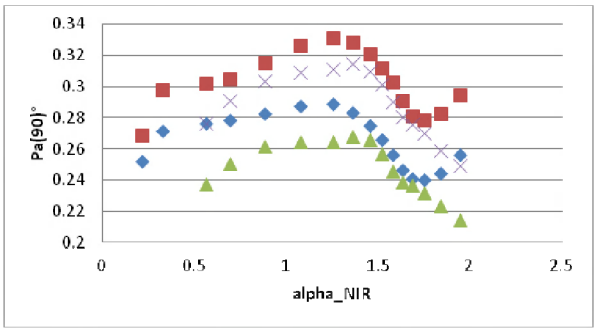

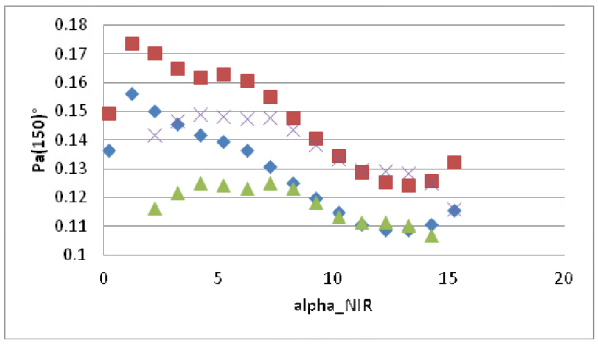

Figure 4: Comparison of Pa versus the Angstroem coefficient $\alpha(670,870)$ with the mean value for AAOT (diamond) and for the 2seas(triangle) and the maximum values value for AAOT (square) and for the 2seas(cross)

The similitude between AAOT and the 2seas is even better on ε, figure 5. Therefore, we can certainly combine the two data sets.

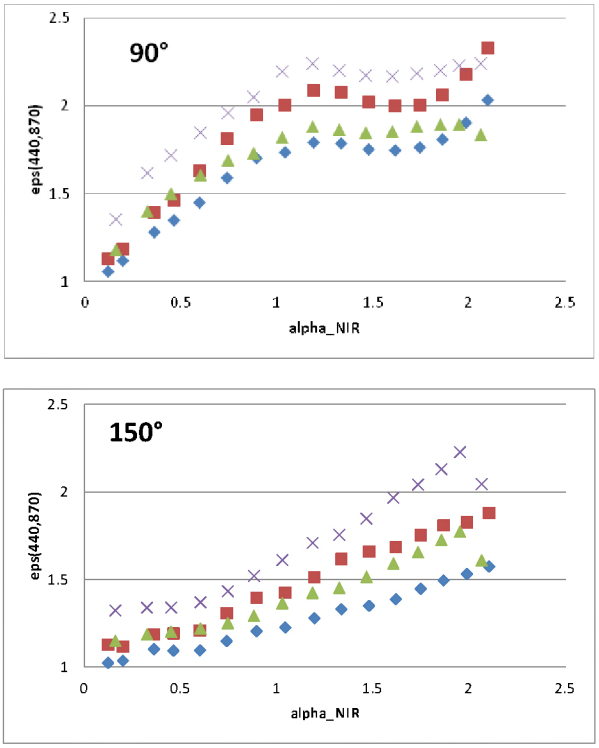

Figure 5: Same as figure 4 but on $\varepsilon(440,870)$

3) THE AEROSOL OPTICAL PROPERTIES FROM WOPAER

3.1) The 2Seas and AAOT data base

We have a WOPAER data base of aerosol optical thickness (AOT) and sky radiance collected to be processed by ourselves by WOPAER. The sky radiance measurements are collected in the principal plane (PP) or in the almulcantar (ALM) at low solar elevation in

order to access to the forward scattering. It is a two step process:

(i) Each individual sky radiance sequence is inverted to obtain P_a at 3 wavelengths. Both the principal plane and the two almulcantars are process at 870 nm and 670 nm.. At 430 nm, only the almulcantar is processed because this geometry is quite insensitive to the vertical distribution of the aerosols, a key parameter in the blue because of the strong influence of the molecular scattering.

(ii) All the inverted P_a are distributed in the 16 classes as in §2.2. Then, all P_a are first averaged and second we apply a filtering based on the relative difference between each sequence and the mean at 83 scattering angles; If for one angle, the relative difference is larger than 50 percent, we reject the sequence.

Table 6 gives for each AERONET station the number of individual measurements processed as described above. It first reflects the climatology of the coastal aerosols (N0) with a clear peak around $\alpha=1.7$. Because of that, the first classes are empty. For the two sites, we have a total o 2109 compared to 9021 of Tab. 1. This difference is explained by the WOPAER selection of low solar elevations. N1 is rather small first because only the almulcantar is inverted and second the inversion is problematic at large view angles. Nevertheless, if we have in mind that AEROPA only produces good inversion when ω_0 is retrieved, *N2=1252* of Tab. 1 as to be compared to a total *N2=1716* of Tab. 6. In other word, the two sets are comparable.

	α	N0	N1	N2	N3	N0	N1	N2	N3
1	0.00	0	0	0	0	0	0	0	0
2	0.15	0	0	0	0	1	1	1	1
3	0.30	0	0	0	0	1	1	1	1
4	0.45	1	0	1	1	0	0	0	0
5	0.60	5	0	5	5	4	3	4	4
6	0.75	16	2	11	12	8	4	7	7
7	0.90	23	2	13	15	12	4	8	11
8	1.05	30	7	20	23	25	14	18	23
9	1.20	57	9	47	47	51	26	37	48
10	1.35	78	12	63	60	104	53	83	90
11	1.50	142	32	103	106	197	112	172	175
12	1.65	199	44	152	157	253	153	220	223
13	1.80	229	41	187	187	211	132	179	185
14	1.95	198	33	162	168	108	67	99	105
15	2.10	95	24	76	82	28	14	25	28
16	2.25	31	4	20	26	2	0	2	2
all		1104	210	860	889	1005	584	856	903

Table 6:_Number of WOPAER sequences at each o the 16 classes (plus the total) for AAOT (left block) and the 2Seas region (right block) with N0: number of sequences before filtering; N1, N2, N3 number of sequences after filtering respectively at 412 nm, 670 nm and 870 nm.

The first comparison brings on the AOT through α, Fig. 6. The 2 regions and the two sets are identical except when few individuals are present in a given class.

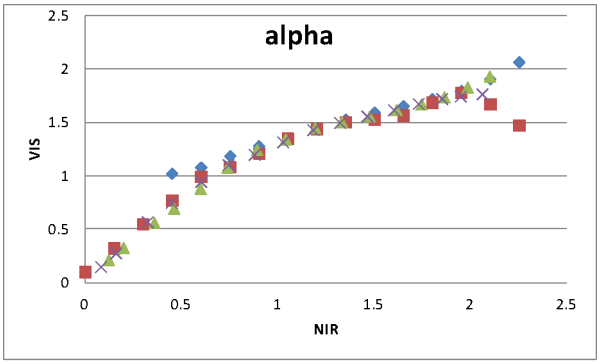

Figure 6: α(670,440) versus α(870,670) for AEROPA at AAOT(cross) and 2Seas (square) and for WOPAER at AAOT(diamond) and 2Seas (triangle)

Fig. 7 gives a comparison between *AEROPA* and *WOPAER* for the single scattering albedo at AAOT; but the same behaviour exists in 2Seas. Let's forget the two first classes for AEROPA and α below 0.75 for WOPAER because the number of sequences we have is not representative. WOPAER indicates a substantial absorption in the red at 670 nm which does not exist in the blue and in the NIR. We carefully checked the WOPAER outputs in this spectral band mainly to see is no trend exist with the AOT. It is not the case. This surprising result has to be understood.

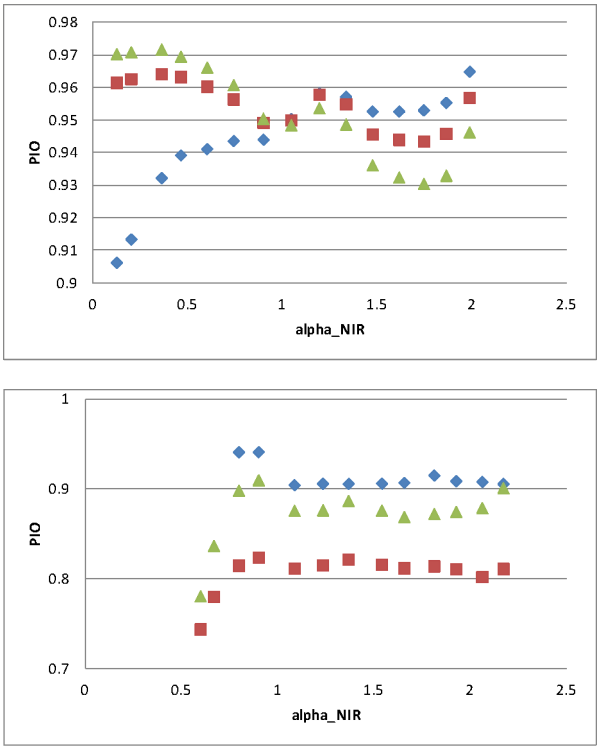

Figure 7: Single scattering albedo at AAOT from AEROPA (upper plot) and WOPAER (lower plot) at 3 wavelengths: 440 nm (diamond), 670 nm(square), 870 nm(triangle)

The similarity between *AEROPA* and *WOPAER* exists on the spectral behaviour of P_a at a scattering angle of *90 deg*. Nevertheless, substantial differences remain in absolute values.

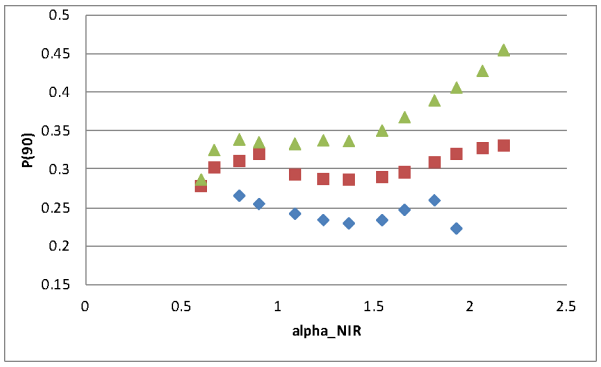

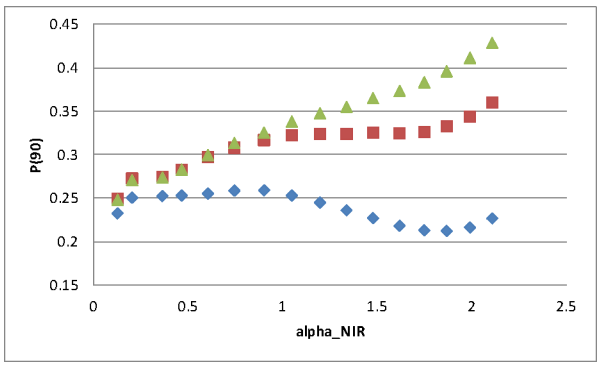

Figure 8: Same at Fig. 7 but for P_a at 90 deg. scattering angle.

4) FROM MERIS TO S3

4.1) The bi-directionality

We clearly see in Fig. 1 the dispersion of P_a. The synergy between MERIS and AATSR (and in S3 between OLCI and SSTS) will offer the opportunity to observe the ocean at two view angles. In the NIR over the black ocean, after gaseous absorption and Rayleigh corrections, we have the aerosol reflectance values and quasi directly the ration between P_a in these two directions. We plotted this ratio in Fig. 9 and the dispersion is such that it will be difficult to derive suitable information on the bi directionality.

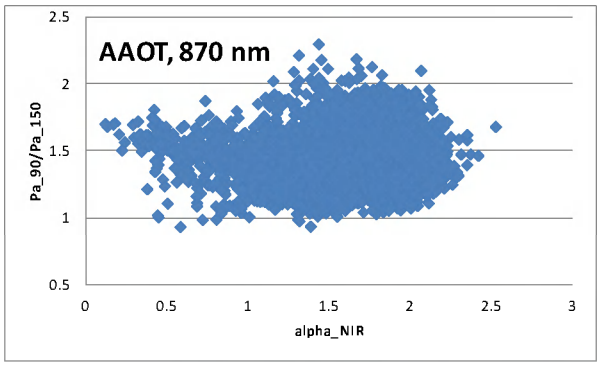

Figure 9: Ratio on Pa at 870 nm between 150 deg. and 90 deg. scattering angles from the AEROPA data base in AAOT.

4.2) The backward scattering

The tilt of OLCI towards the West in order to avoid the sunglint, will increase the occurrence to observe in backscattering. From the Mie theory P_a computations, we know that the backscattering is very sensitive to the size distribution as well as to the refractive index. This sensitivity is pronounced for larges aerosols as foreseen to be representative of the open ocean. Here, we have a sample more representative of the coastal waters. We did not report the dispersion of Pa as we did in Fig. 1, but it is quite identical at large scattering angles. Instead, we plot *ε(440,870)*, Fig. 11. Clearly, the uncertainty in the extrapolation from the NIR to the blue increases in backscattering.

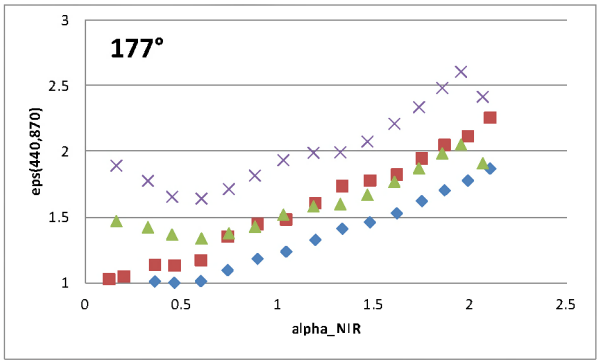

Figure 11: Same as Fig. 5 but for a scattering angle of 177deg..

4.3) The error bars

One request is to have error bars on the water reflectance values after atmospheric correction. In an analytical approach, the error bars can be directly derived from the ADF. The inputs to the ADF generation are the P_a and from the approach we conducted, we have can put the error bars on P_a. The straightforward strategy is then to generate three sets of ADF: mean, max and min and to use them with the same algorithm. That what we did and will report in a companion paper

5) CONCLUSION

We first evaluated two different uses of the AERONET data. The advantages of AEROPA is to be stamped by NASA which means: important effort in developing the algorithms and document them, integration in an operational processing chain with quality control, public access and many feedback from the scientific community. The disadvantage is the need to rely on *a priori* assumption on the shape of the aerosols, their composition,... Also, the inversion is mostly based on the forward scattering and on the spectral dependence of the AOT. The first advantage of WOPAER is to convert the sky radiance into *Pa* with few physical

assumptions (aerosol vertical distribution, contribution of the surface) and an expected limited impact on those assumptions because they are also used in the generation of the ADF. The second advantage of WOPAER is to use in priority the forward scattering, a geometry shared by the observations from space. The disadvantage of the two methods is the impossibility to access experimentally to the near backscattering (scattering angles larger than 150°).

The natural variability of the aerosol combined to the uncertainty of each method result in substantial errors in the retrieval of P_a or on the spectral dependence of the aerosol reflectance. The dispersion is more pronounced for small aerosols, which renders the atmospheric correction more challenging in coastal areas where they are compared to the open ocean. Within the dispersion, the two methods compared quite well as soon as a given class possesses a representative number of elements. The exception is the quite small SSA at 670 nm that WOPAER reports. Further checking of the result and a deeper analysis are required.

The dispersion of P_a suggests that a validation of the aerosol product restricted to the use of the AOT measurements may be not suitable. The measurement of P_a during matchups is required. This aspect is reported in a companion paper.

After the characterization of the aerosol IOPs, it is necessary to build an aerosol climatology in the context of the ADF generation. What we see in our analysis is first that the aerosol IOPs do not vary much from the south-western North Sea to the Adriactic Sea and second that seasonal effects are within the error bars.

A climatology driven by the micro-physic presents a risk in the continuity of the IOP versus the spectral dependence of the aerosol reflectance. It was the case for the MERIS SAM when the two bracketed models do not belong to the same family (maritime, urban,..). Than the reason why, we prefer to organize the data base with the IOP. All our plots versus $\alpha(670,870)$ indicated that this continuity exist.

The dispersion in each class is quite large. In order to reduce it, we investigated the bi-directionality provided by AATSR which seems to bring nothing. One clear possibility lies in the polarisation. Some CIMEL radiometers are equipped, enough to investigate this opportunity. One other possibility is to extend the spectral range. The new CIMEL radiometers have a spectral bands at 1.65 µm!

We clearly have the inputs to produce error bars on the retrieval of the water reflectance values from space. We will see the results but we can already suspect that this task is difficult in coastal waters.

6) BIBLIOGRAPHY

1. Holben, B., T. Eck, I. Slulutsker, D. Tanré, J.P. Buis, A. Setzer, E. Vermote, J. Reagan, Y. Kaufman, T. Nakajima, F. Lavenu, I. Jankowiak, and A. Smirnov, 1998. "AERONET – A federated instrument network and data archive for aerosol characterization", *Remote Sensing of Environment*, **66**, pp. 1-16.

2. Santer, R., F. Zagolski, and O. Aznay, 2009. "Aerosol phase function derived from CIMEL measurements", *International Journal of Remote Sensing*, **31** (4), 969-992 (*doi:10.1080/01431160902912087*).

3. Dubovik, O., and M.D. King, 2000. "A flexible inversion algorithm for retrieval of aerosol optical properties from Sun and sky radiance measurements", *Journal of Geosphysical Research*, **105**: 20673–20696.

4 O. Aznay, F. Zagolski, and Santer, R.,(2011) 'A new climatology for remote sensing over land based on the inherent optical properties', International Journal of Remote Sensing, 32: 10, 2851 — 2885.

5., F. Zagolski, Santer, R and O. Aznay,(2007). A new climatology for atmospheric correction based on the aerosol inherent optical properties**.** Journal of Geophysical Research, *Vol. 112, No. D14, D14208*

6 Ahmad, Z., B.A. Franz, C.R. McClain, E.J. Kwiatkowska, J. Werdell, E.P. Shettle, and B.N. Holben, 2010. "New aerosol models for the retrieval of aerosol optical thickness and normalized water-leaving radiances from the SeaWiFS and MODIS sensors over coastal regions and open oceans", *Applied Optics*, **49** (29): 5545-556

7 F. Zagolski, Santer, R., and O. Aznay, Apparent Optical Properties of the Aerosols for MERIS/OLCI-S3: Selection of best LUTs for Atmospheric Correction over Ocean. This proceeding.

8 O. Aznay Santer, R.and, F. Zagolski. Validation of the MERIS Atmospheric Correction over Ocean using AERONET. This proceeding.

7) ACKNOWLEDGMENTS

We thanks all the PIs for the AERONET stations we used: G. Zibordi for the AAOT, K. Ruddik for Oostende, R. Doorfer for the Helgoland, B. Holnen for Lannion, P.Goloub for Dunkerque.

This work was partially supported by the INTERREG 2 Seas program.